Evidence of low intermolecular coupling in rubrene single crystals by Raman scattering

2007 J. Phys.: Condens. Matter 19 276204

(http://iopscience.iop.org/0953-8984/19/27/276204)

IOP PUBLISHING JOURNAL OF PHYSICS: CONDENSED MATTER

J. Phys.: Condens. Matter **19** (2007) 276204 (15pp) doi:10.1088/0953-8984/19/27/276204

Evidence of low intermolecular coupling in rubrene single crystals by Raman scattering

J R Weinberg-Wolf[1], L E McNeil[1], Shubin Liu[2] and Christian Kloc[3]

[1] Department of Physics and Astronomy, University of North Carolina at Chapel Hill, Chapel Hill, NC 27713, USA
[2] Division of Research Computing, Information Technology Services, University of North Carolina, Chapel Hill, NC 27713, USA
[3] Bell Laboratories, Lucent Technologies, 600 Mountain Avenue, Murray Hill, NJ 07974, USA

Received 20 March 2007, in final form 31 May 2007
Published 20 June 2007
Online at stacks.iop.org/JPhysCM/19/276204

Abstract

The observed Raman spectra for single crystals of rubrene and tetracene are compared with the calculated spectra for the isolated molecules. The Raman measurements presented are of the bulk properties of the material, and they confirmed that the vapour growth process yields very pure, unstrained rubrene crystals. Finally, Raman measurements indicate that rubrene, unlike many other oligoacenes, has very weak intermolecular coupling and no observable intermolecular Raman vibrational modes. We discuss the apparent conflict between the high mobility and the weak π-electron overlap in this material.

1. Introduction

Within the last 50 years, interest in the optical properties of organic molecular crystals has grown. Many books and reviews of interesting optically active materials are available in the literature [1, 2]. Once the first organic light-emitting device (OLED) was successfully fabricated using thin films of 8-hydroxyquinoline aluminium (Alq_3) in 1987 [3], interest in the applications of these optically active organic molecular materials has grown, opening the door for the development of a new commercial product: all-organic displays based on OLEDs and organic field-effect transistors. A good review of the work on thin-film technology using organic materials was published recently by Horowitz [4]. The first single-crystal organic semiconductor field-effect transistor (FET) [5], which used α-hexathiophene, followed soon after the thin-film device work. Compared to liquid crystal display (LCD) technology, organic transistors and discrete LED displays hold the potential for devices with improved characteristics, including lower power requirements, better resolution, more mechanical flexibility, and lower production costs (to name just a few benefits). Research to date has focused on two distinct directions: semiconducting polymers and organic small molecules. The former may have the advantage of higher stability for practical applications, but the latter, due to the feasibility of forming large single crystals, seems to be more suitable

for basic science studies. Small molecules with high levels of conjugation are particularly appealing for display applications as the typical highest occupied/lowest unoccupied molecular orbital (HOMO/LUMO) separation is in the visible range. Consequently, they can be used for a host of photonic devices. Some of these molecules are also very stable, another requirement for a successful device. Many different molecules have been studied and numerous devices created [6, 7]. An understanding of the relationships among crystal structure, optical properties, and transport properties of a material is crucial to advance design possibilities. The hope is that, once this connection is well understood, it will be possible to tailor molecules for desired performance in devices.

Certain molecules with high carrier mobilities (for organics) have garnered much attention recently. Among the leading candidates for detailed investigation are α-hexathiophene, pentacene, rubrene (5,6,11,12-tetraphenyl tetracene) and others. This study focuses on single crystals of rubrene and tetracene. Rubrene has an almost 100% photoluminescent yield [8], and it has been successfully doped into many other OLED devices to improve their characteristics, such as lifetime [9], stability [10], colour [11], and brightness [12]. It has also been used in other devices, including chemical sensors [13] and actinometers [14]. The hole mobility of rubrene has been reproducibly measured at many laboratories. Researchers have found an FET mobility [15] as high as 20 $cm^2\ V^{-1}\ s^{-1}$ at room temperature, which is even higher than that of amorphous hydrogenated silicon. Also, time of flight measurements of the hole mobility in rubrene [16] indicate values as high as 2 $cm^2\ V^{-1}\ s^{-1}$. Much less is known so far about the electronic and vibrational structure of the crystal. Studies of (relatively defect-free) single crystals allow us to learn about the intrinsic characteristics of the material and shed light on the exceptionally high mobility of rubrene in comparison to other acenes.

Raman spectroscopy is a non-destructive characterization method that probes the vibrational modes of a crystal. Theoretical calculations can also be performed on the single molecule to predict the vibrational spectrum. Comparing the experimental and theoretical spectra of different crystals (like rubrene and tetracene in the present study) can yield insight into the electron–phonon interaction in the solid state, and hence indirect information about the electronic properties of the crystal that are important for devices, especially the very high electron mobility.

2. Experiment and simulation

Rubrene is a relatively small aromatic hydrocarbon consisting of a backbone of four fused benzene rings (tetracene) with four substituted phenyl groups (two on each internal ring) as shown in figure 1. Steric hindrance dictates that the substituted phenyl groups are rotated out of the plane of the tetracene backbone.

The single crystals used in these measurements were grown at Bell Laboratories by horizontal physical vapour transport in a flow of argon gas from rubrene powder acquired from Aldrich. The details of this growth process for similar materials [17] and for rubrene [18] have been described elsewhere. To change the morphology of the growing crystals and to get thick bulk crystallites more suitable for this present study, some previously sublimed rubrene crystals were subsequently used for a typical vacuum-sealed ampoule growth. The molecule crystallizes in an orthorhombic structure and has D_{2h}^{18} point group symmetry [19] with four molecules per unit cell. The lattice constants for the orthorhombic unit cell are $|a| = 14.430$ Å, $|b| = 7.187$ Å, and $|c| = 26.901$ Å. The molecular stacking in the crystal is shown in figure 2. Most crystallites are thin or thick platelets, millimetres in lateral dimension. The face of the crystallites is the *bc*-plane. The consensus from the literature is that the crystals have a room-temperature band gap of approximately 2.21 eV [20].

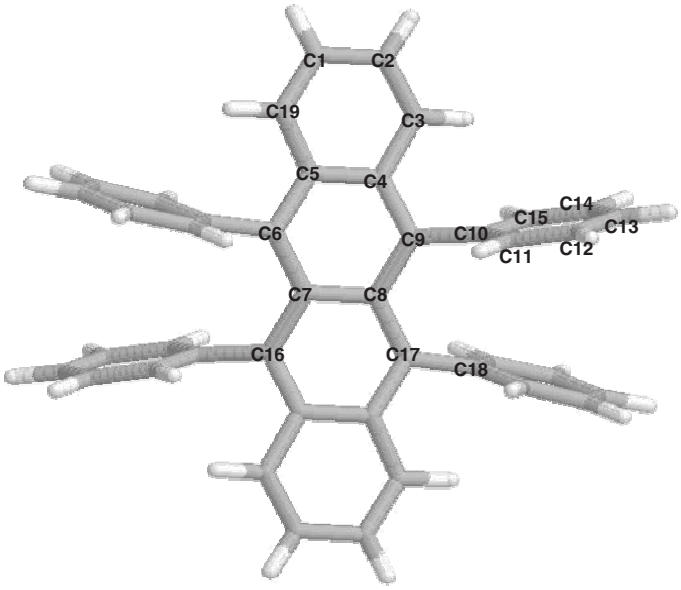

Figure 1. Rubrene ($C_{42}H_{28}$) molecule. The labels on the carbon atoms are in reference to table 1.

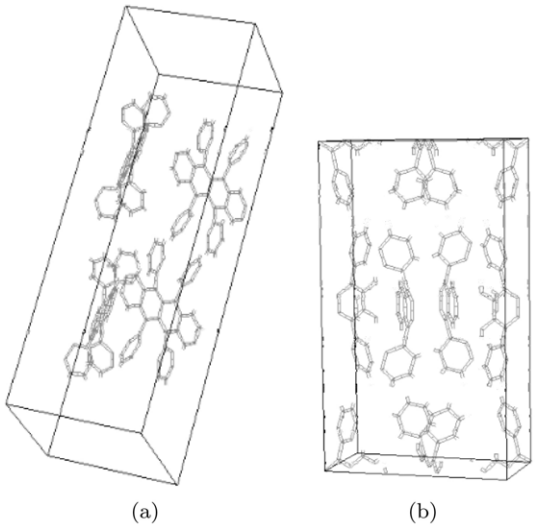

Figure 2. Two views of the packing in rubrene single crystals. (a) shows the orientation of molecules with respect to each other while (b) is the primitive unit cell based on x-ray data.

Multiple crystallites from the same growth batch were mounted at the same time for the initial experiment. No deliberate attention was paid to the orientation of the crystallites at the time of mounting. Any polarization effects will therefore be averaged over the entire group of crystals and must be accounted for in the analysis. Studying multiple crystals also allows us to investigate the consistency of crystals produced in a single growth run. The largest crystallites were selected from multiple growth runs in order to allow for access to different crystal faces, and therefore observation of vibrational modes with different symmetries. Rubrene is known

to highly favour creating a peroxide layer in the presence of light and oxygen [21]. No attempts were made to keep the crystals dry or in the dark, so the room-temperature, ambient-pressure spectra presented here are of both the underlying bulk rubrene crystal and any surface peroxide layer. It is important to remember during the subsequent discussion that the Raman data are of the bulk material, while other interesting attributes of rubrene's high FET mobility are possibly from surface channel conduction, and are therefore affected by oxidized molecules.

Raman spectra were recorded using a Dilor XY triple spectrometer in a backscattering configuration and collected using a charge-coupled device (CCD) cooled with liquid nitrogen (LN_2). The resolution of the spectrometer is 1 cm^{-1}. The crystals were cooled to 20 K with an Air Products closed-cycle He refrigerator in a cryogenic chamber pumped down to approximately 10^{-6} Torr with a diffusion pump vacuum system. A Spectra Physics 2017 Ar^+ laser was used to pump a Spectra Physics 375B dye laser with Kiton Red dye. The output energy of the dye laser is continuously tunable from 608 to 711 nm, but an excitation wavelength of 653.55 nm (1.897 eV) was used in the experiments to minimize the photoluminescence from the sample in order to measure the weaker Raman effect. Data were collected over the spectral range from approximately 35 to 1600 cm^{-1}, a range that would be expected to include both intermolecular and intramolecular vibrations. After subtracting the background, all peaks were fitted using Lorentzian lineshapes with a least-squares algorithm.

The Raman spectra for isolated molecules of rubrene and any possible oxidation molecules were also simulated. The calculations were performed using GAUSSIAN 03 [22]. The Hartree–Fock method was used to do a structural optimization and the density functional theory (DFT) B3LYP method was used to calculate the Raman frequencies, both with the 6-31G* basis set. The calculation with GAUSSIAN 03 was repeated with both the structural optimization and the frequency simulation done with the DFT B3LYP method and the 6-31G9(d) basis set for the isolated rubrene molecule. All calculations were performed on an SGI Origin 3800 with 64 CPUs and 128 GB memory running the IRIX 6.5 operating system.

3. Results and discussion

Overall, a few statements can be made about rubrene based on this Raman investigation. First, the vapour deposition growth process produces very homogeneous crystals within each run. Raman spectra were recorded for a number of crystallites, but no attempt was made to mount the crystals in specific orientations. In Raman spectroscopy, the cross section for scattering depends in part on the scalar product of the incident light polarization, the Raman tensor for a particular mode and the scattered light polarization:

$$\frac{\partial \sigma_s}{\partial \Omega} \propto |\epsilon_s \cdot \widetilde{R} \cdot \epsilon_i{}^2|. \tag{1}$$

In equation (1), $\frac{\partial \sigma_s}{\partial \Omega}$ is the differential scattering cross section, $\hat{\epsilon_s}$ and $\hat{\epsilon_i}$ are the polarizations of the scattered and incident light, respectively, and $\widetilde{R}$ is the Raman tensor for the system. The geometric arrangement of the experimental set up, the polarization of the incident and scattered light and the symmetry of the crystal are therefore important factors in the overall scattering cross section. As previously mentioned, rubrene crystallizes in the D_{2h}^{18} point group, which allows vibrations of eight symmetry types: A_g, A_u, B_{1g}, B_{1u}, B_{2g}, B_{2u}, B_{3g}, B_{3u}. This point group has a centre of inversion, so only the gerade modes are Raman active. The Raman

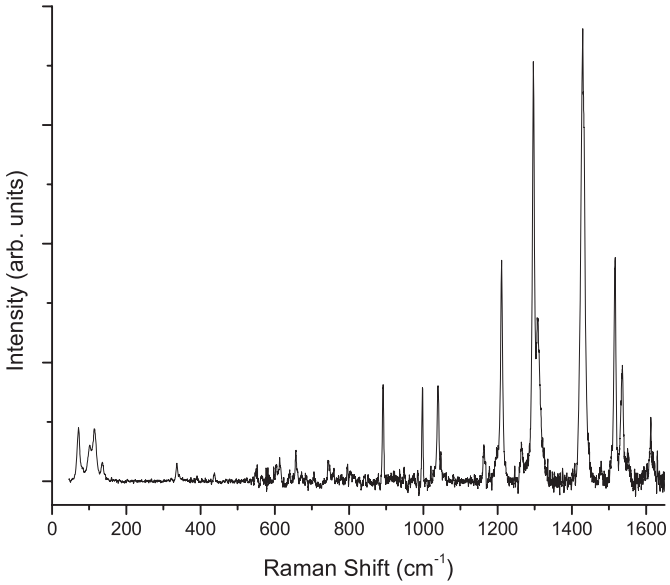

Figure 3. Representative room-temperature Raman spectrum of rubrene single crystals collected with an excitation energy of 653.55 nm (1.897 eV).

tensors for these allowed modes are

$$\mathrm{A_g} = \begin{pmatrix} a & 0 & 0 \\ 0 & b & 0 \\ 0 & 0 & c \end{pmatrix} \qquad \mathrm{B_{1g}} = \begin{pmatrix} 0 & d & 0 \\ d & 0 & 0 \\ 0 & 0 & 0 \end{pmatrix}$$
$$\mathrm{B_{2g}} = \begin{pmatrix} 0 & 0 & e \\ 0 & 0 & 0 \\ e & 0 & 0 \end{pmatrix} \qquad \mathrm{B_{3g}} = \begin{pmatrix} 0 & 0 & 0 \\ 0 & 0 & f \\ 0 & f & 0 \end{pmatrix}. \tag{2}$$

Most of the rubrene crystals have the *bc* plane available in many different orientations in this experiment. In a backscattering configuration, only $\mathrm{A_g}$ and one of the $\mathrm{B_g}$ modes can be observed. Depending on the relative orientation of the crystal axes in the face of the crystallites and the incident polarization, one would expect that only the relative intensities of the $\mathrm{A_g}$ mode and one $\mathrm{B_g}$ mode should change. Raman spectra were collected from ten different platelet-like crystallites (as well as from multiple locations on some of the larger crystallites). All of the spectra are substantively the same, other than small changes in the relative intensities of individual peaks, as predicted by group theory arguments. This is a strong indication that the crystal-growing process is creating only very pure, unstrained rubrene crystals. Figure 3 is a representative Raman spectrum measured from the different crystallites.

More information about the individual modes can be gained from the spectra, especially when compared to calculations of Raman modes of both rubrene and the backbone molecule tetracene. Table 1 lists the atomic positions and the bond angles from the geometric minimization of the rubrene molecule. X-ray measurements of these crystals show that their structure agrees with that previously published for rubrene [23] and tetracene [24] (discussed later in this paper). As mentioned previously, two calculation runs with GAUSSIAN 03 were performed on the isolated rubrene molecule. The second calculation required much more CPU time, but there is virtually no difference between the two simulated spectra for almost every higher-energy mode. For the low-energy modes, only small differences appeared: the lowest-energy mode at about 21 $\mathrm{cm^{-1}}$ upshifted 13%, the other low-energy modes upshifted 3% or

Table 1. Comparison of experimental and theoretical geometrical structures of rubrene and tetracene molecules. Refer to the atomic labelling scheme in figure 1.

	Rubrene		Tetracene	
	Experiment[a]	Theory	Experiment[b]	Theory
Distances				
C1–C2	1.442 Å	1.408 Å	1.431 Å	1.420 Å
C2–C3	1.366 Å	1.351 Å	1.367 Å	1.365 Å
C3–C4	1.439 Å	1.433 Å	1.434 Å	1.427 Å
C4–C5	1.466 Å	1.440 Å	1.452 Å	1.452 Å
C7–C8	1.474 Å	1.464 Å	1.452 Å	1.455 Å
C8–C9	1.431 Å	1.418 Å	1.410 Å	1.395 Å
C4–C9	1.409 Å	1.397 Å	1.393 Å	1.391 Å
C9–C10	1.503 Å	1.506 Å	N/A	N/A
C10–C11	1.402 Å	1.385 Å	N/A	N/A
C11–C12	1.395 Å	1.386 Å	N/A	N/A
Angles				
C3–C4–C9	121.8°	122.4°	122.3°	122.3°
C4–C9–C10	116.0°	115.6°	N/A	N/A
C8–C9–C10	122.9°	123.1°	N/A	N/A
C9–C8–C17	122.2°	122.3°	N/A	N/A
C10–C9–C17–C18	29.4°	25.1°	N/A	N/A

[a] See [23].
[b] See [24].

less, and the rest of the intramolecular modes changed less than 1% with the higher-level basis set calculation.

There is a one-to-one correspondence between the calculated spectrum for the isolated molecule and the observed Raman spectra for the single crystal. The positions of the peaks in the calculated spectrum for the isolated molecule, when plotted against the positions from the experimentally measured spectrum from the single crystal, lie along a least-squares fit line with a slope of 0.997 and a correlation coefficient of 0.9994. Overall, for modes of frequency greater than 300 cm^{-1}, the calculated peak energies are within 2% of the experimentally observed energies after the typical scaling factor [25] of 0.96 has been applied to the theoretical frequencies. The lower-energy modes are farther from experimental values for two main reasons. Mathematically, small errors at low frequency simply appear large when given as percentages. Errors as large as 20% correspond to shifts of only 10–20 wavenumbers. Physically, one would expect lower-energy modes to be affected more by crystal forces (van der Waals bonding between molecules) than higher-energy modes. As the simulation is for a single molecule, rather than the measured single crystal, it is not surprising that the theory and experiment diverge more here. For each CCD window, the peaks in the experimental spectrum were scaled so that the tallest experimental peak matched the intensity of the corresponding theoretical peak. This scaling technique resulted in intensities that matched within a factor of two between the experimental and theoretical spectra.

The one-to-one correspondence between peaks in the calculated and observed spectra, and the close correlation in energy of these peaks of the molecule and single crystal allows us to use the theoretically predicted symmetries of molecular modes to identify the symmetries of the single crystal Raman modes, as listed in table 4. Even though the isolated rubrene molecule has C_{2h} point group symmetry, rather than the D_{2h} of the crystal, A and B modes in the molecular

Table 2. Irreducible representation for the isolated rubrene molecule.

E	C_2 (y)	i	σ_{xz}
210	−2	0	0

Table 3. Character table for the C_{2h} point group.

	E	C_2	i	σ_h
A_g	1	1	1	1
B_g	1	−1	1	−1
A_u	1	1	−1	−1
B_u	1	−1	−1	1

spectrum retain their symmetry type in the crystal. A close inspection of figures 1 and 2 reveals that part of a rubrene molecule lies along a mirror plane in the primitive unit cell. Therefore, a mode that was initially symmetric with respect to the axis of symmetry (A_g) in the isolated molecule would still have to be symmetric with respect to a mirror plane in the single crystal. A detailed group theory analysis of the molecule allows the calculation of the number of each symmetry mode once the irreducible representation (see table 2) and the character table (see table 3) for the C_{2h} point group are known. From this analysis we predict 51 A_g, 51 B_g, 51 A_u and 51 B_u modes, exactly the same distribution of modes from the theoretical simulations.

Additional insights in the interpretation of the rubrene single-crystal spectrum can be gleaned from comparing it to the Raman spectra from similar molecules, such as tetracene. Rubrene is composed of a tetracene backbone with four substituted benzene rings. These benzene rings do not disrupt the conjugation or bonding of the tetracene backbone. Therefore, one would expect great similarities between the vibrational modes of rubrene and tetracene. As there is a lack of a high-quality single-crystal spectrum of tetracene in the literature [26, 27], we have measured and calculated the Raman spectrum of tetracene for the purpose of comparing it with the Raman spectrum of rubrene. Figure 4 is the measured Raman spectrum for tetracene single crystals. The slope of the least-squares fit of the positions of the calculated and measured tetracene modes is 1.008 with a correlation coefficient of 0.9995, showing once again how well the theory matches the experimental spectrum. Tetracene and rubrene have substantially different Raman spectra, as can be seen by comparing figures 4 and 3. Before comparing the tetracene and rubrene spectra, a short discussion of the tetracene spectrum is beneficial.

The correspondence between the simulated isolated single-molecule spectrum and the measured single-crystal spectrum is not nearly as close as that of rubrene. There are two important reasons for this. First, tetracene is a rigid, planar molecule that can pack very tightly. Tetracene crystallizes with triclinic C_i symmetry with two molecules in the unit cell. The lattice parameters are 7.98, 13.57, and 6.14 Å [28], while the lattice parameters of rubrene are 14.43, 7.19, and 26.9 Å [19, 29]. The primitive unit cell of rubrene is more than four times as large as that of tetracene. While the molecule itself is larger than tetracene, and there are four rather than two molecules in the unit cell, the change in the volume of the unit cell is also due to differences in packing. The phenyl groups on the rubrene molecule prevent the close-packing arrangement achieved by tetracene in the solid state. The molecules in a rubrene crystal are nearly three times farther from each other than are those in the tetracene crystal; the packing densities for both rubrene and the other oligoacenes can be found in table 7. For this reason, it is not surprising to find much stronger intermolecular interactions between tetracene molecules, and hence a larger difference between the simulated isolated molecule spectrum and the measured single-crystal spectrum. These intermolecular interactions affect the crystal spectrum in two

Table 4. Peak positions for the measured and calculated Raman spectra of rubrene, including symmetry assignments from the theoretical calculations—B_g modes from the isolated molecule spectrum are one of the B_g modes in the single-crystal spectrum for the platelet crystals and either of the other two possible B_g modes found on the other crystallite faces of the larger three-dimensional (3D) crystal. A full listing of all the theoretically calculated peaks and their symmetries can be found at http://www.physics.unc.edu/project/mcneil/MolecularAnimations/anim.php.

	Position (cm^{-1})		Comparison
Symmetry	Theory[a]	Experiment	Difference (%)
B_g	72.2	73.7	2
B_g	80.3	85.7	6.3
A_g	83.2	107.0	22.2
B_g	96.5	120.3	19.8
A_g	128.6	141.7	9.2
A_g	205.3	204.4[b]	0.4
A_g	254.4	236.6[b]	7.5
A_g	326.4	342.0	4.6
B_g	385.4	393[b]	1.9
B_g	467.7	470[b]	0.5
A_g	514.1	517[b]	0.5
B_g	575.3	613.7	6.2
A_g	872.8	896.3	2.6
A_g	977.7	1003.9	2.6
A_g	1026.6	1046.0	1.9
A_g	1183.9	1163.0	−1.8
B_g	1251.1	1268.2	1.4
A_g	1295.1	1299.9	0.4
A_g	1307.1	1310.9	0.3
B_g	1330.5	1315.7	−1.1
A_g	1420.8	1432.3	0.8
B_g	1487.7	1519.9	2.1
A_g	1530.4	1539.9	0.6
A_g	1592.3	1616.8	1.5

[a] Additional peaks were calculated to be at 22.9 and 67.2 cm^{-1} but this is outside the range of the measured spectrum.
[b] From 3D crystallite experiment.

ways: by the presence of new, low-energy intermolecular vibrational modes and by the lifting of degeneracies of higher-energy intramolecular modes, both of which are seen in a comparison of the two spectra. The splitting of peaks could be due to crystal-field splitting like Davydov splitting, or the vibronic mixing of different molecular states. An analysis of the energy split versus temperature would be necessary to distinguish these two possibilities.

The authors believe that all the modes observed in tetracene below 200 cm^{-1} are, in fact, intermolecular vibrational modes, and are therefore not predicted in the isolated molecule simulation. The tetracene crystal has two molecules in the unit cell; therefore, all molecular modes could be split into doublets by interactions in the solid state. While not every doublet can be resolved in the experimental data, all the frequencies (including all members of each pair) of the higher-energy modes are within 1.3% of a scaled predicted mode. Table 5 lists the correspondence between the experimentally observed intramolecular modes and those predicted by the theoretical simulations. Every calculated mode with a scaled intensity above the noise of the experiments has a corresponding experimentally observed mode, indicating the strong correlation between the theory and the experiment. Given this correspondence, one

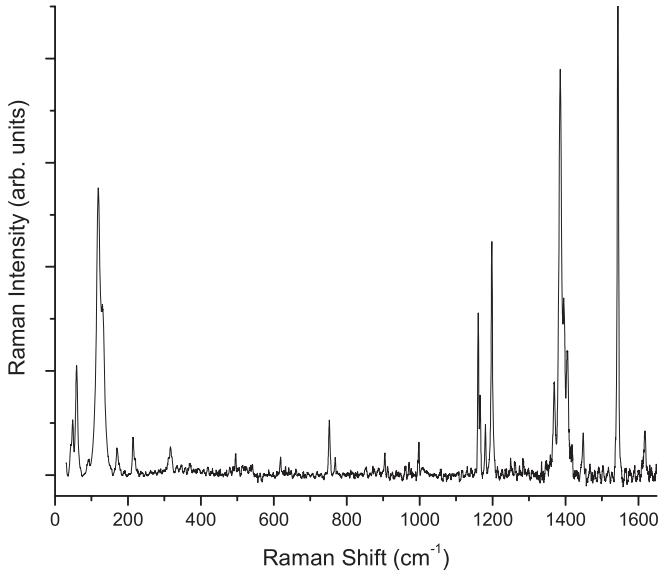

Figure 4. Room-temperature Raman spectrum of tetracene single crystals collected with an excitation energy of 653.55 nm (1.897 eV).

Table 5. Frequency of intramolecular modes for tetracene, both experimentally measured for the single crystal and calculated for the isolated molecule.

	Position (cm^{-1})		Comparison
Symmetry	Theory[a]	Experiment	Difference(%)
B_{1g}	146.0	130.7	11.7
A_g	305.8	316.1	−3.3
B_{3g}	484.8	495.0	−2.1
A_g	735.2	752.2	−2.3
B_{2g}	748.8	768.3	−2.5
A_g	990.9	998.1	−0.7
B_{3g}	1168.5	1160.5	0.7
		1165.9	0.2
A_g	1190.1	1180.2	0.8
		1197.8	−0.6
A_g	1370.6	1368.8	0.1
		1386.0	−1.1
A_g	1384.6	1395.6	−0.8
A_g	1438.1	1403.5	−1.3
		1448.1	−0.7
A_g	1529.6	1543.0	−0.9
		1544.7	−10
B_{3g}	1596.9	1617.5	−1.3

can use other information from the theoretical predictions to help interpret the experimental spectrum: specifically the symmetry assignments of the actual modes and the atomic motions they represent. Included in table 5 are the symmetries of the modes from the theoretical predictions.

Since the rubrene molecule is just a derivative of the tetracene molecule, it should be possible to categorize some of the vibrational modes of rubrene as derived from modes of tetracene. Our theoretical calculations yield individual displacement vectors per atom per normal mode of vibration. These calculations have been turned into animations that can be viewed as individual movies at http://www.physics.unc.edu/project/mcneil/MolecularAnimations/anim.php. Viewing these animations allows us to understand the motions involved in different vibrational modes and compare them with those of tetracene. For example: the rubrene mode at 1157.9 cm^{-1} involves a scissor motion of the terminal hydrogen of the backbone; the tetracene mode at 1147.6 cm^{-1} involves the same motion.

The comparison of the spectra of these two molecules reveals a more significant finding: the strikingly small intermolecular coupling of rubrene. In most molecular solids, Raman modes below about 150 cm^{-1} are almost always intermolecular modes. However, the Raman spectrum for the isolated rubrene molecule predicts many low-energy modes in this region and the one-to-one correspondence with the experimental spectrum indicates that the lowest-energy modes measured here are, in fact, all intramolecular. In stark contrast to this is the predicted spectrum for the isolated molecules of tetracene. In that instance there are basically no modes predicted below 300 cm^{-1}, but many are observed experimentally. This contrast between the low-energy theoretical and experimental spectra for rubrene and tetracene is very evident in figure 5. Figure 6 further highlights the differences between rubrene and tetracene single crystals. Both parts of figure 6 show the correspondence between experimentally measured and theoretically predicted peaks in the Raman spectra. In both figures the correspondence between the theory and experiment is very high, as each line has a slope of nearly one. However, the insets, which zoom into the low-energy region of each spectrum, are very different. There is only one theoretically predicted tetracene peak below 200 cm^{-1}, whereas there are six theoretically predicted rubrene peaks in the same region. As the theory is for the isolated molecule, it cannot predict intermolecular modes—vibrations associated with motions between neighbouring molecules.

A very obvious difference between intermolecular and intramolecular modes can be found in their temperature dependence. Intermolecular modes associated with vibrations of the atoms bound by the weaker van der Waals forces are disproportionately affected by changes in temperature compared to the stronger covalent bonds that stretch in intramolecular vibrational modes because temperature changes cause changes in the lattice constants. In fact, when the rubrene crystallites are cooled from room temperature to 20 K, there is only a small upshift in the Raman signal. These modes are changing by less than 3% (see figure 7 or table 6), whereas intermolecular modes of other organic molecular crystals change more. In crystalline C_{60} the energy of the strongest intermolecular mode changes by 30% over the temperature range of 258–10 K [30]. Between the small temperature dependence and the strong correlation with the theory that cannot predict intermolecular modes, we are led to conclude that all the observed vibrational modes of rubrene are intramolecular in nature. This lack of strong intermolecular modes and the close correspondence between the isolated single molecule and the crystal show the weak coupling between molecules in the solid state of rubrene.

In a molecular crystal, intermolecular coupling influences the carrier mobility. On the one hand, low vibrational coupling between molecules helps explain the large mobility of rubrene because the mean free path of an electron should be larger in rubrene than other organic molecular crystals with fewer intermolecular phonons that can scatter electrons. On the other hand, the low vibronic coupling indicates small π-electron overlap between the molecules. Molecular crystals that have tight packing, and hence more overlap, tend to have a higher mobility. This trend can be seen by comparing the rigid oligoacenes. As the number of phenyl rings in the backbone is increased, the density of the crystal increases, and at the same time, the

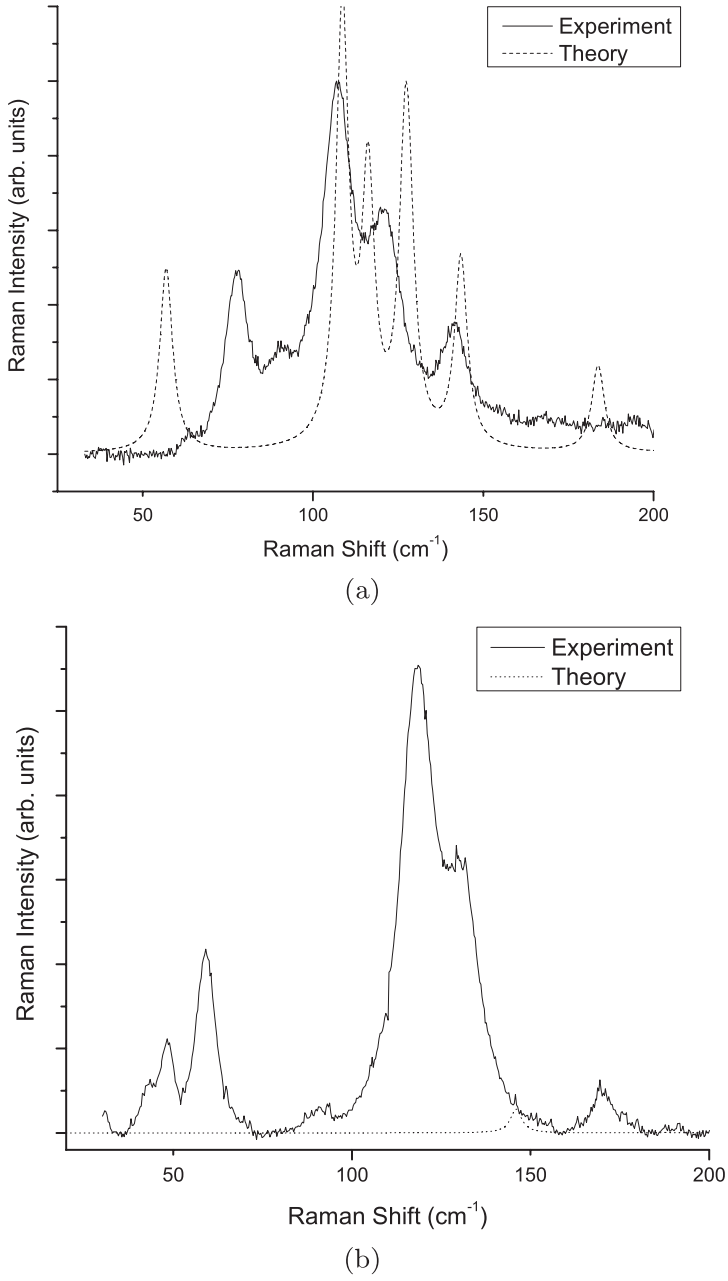

Figure 5. Room-temperature low-energy experimental data and theoretical predictions for (a) rubrene and (b) tetracene single crystals.

mobility increases, as listed in table 7. The trend of increasing mobility with chain length is much clearer from the theoretical predictions; experimental results do follow this trend, but it is clear from an investigation of the literature that crystal preparation and purity are as important (if not more important) than the actual composition in determining the mobility. A recent calculation of the interchain transfer integrals in rubrene suggest that the packing of

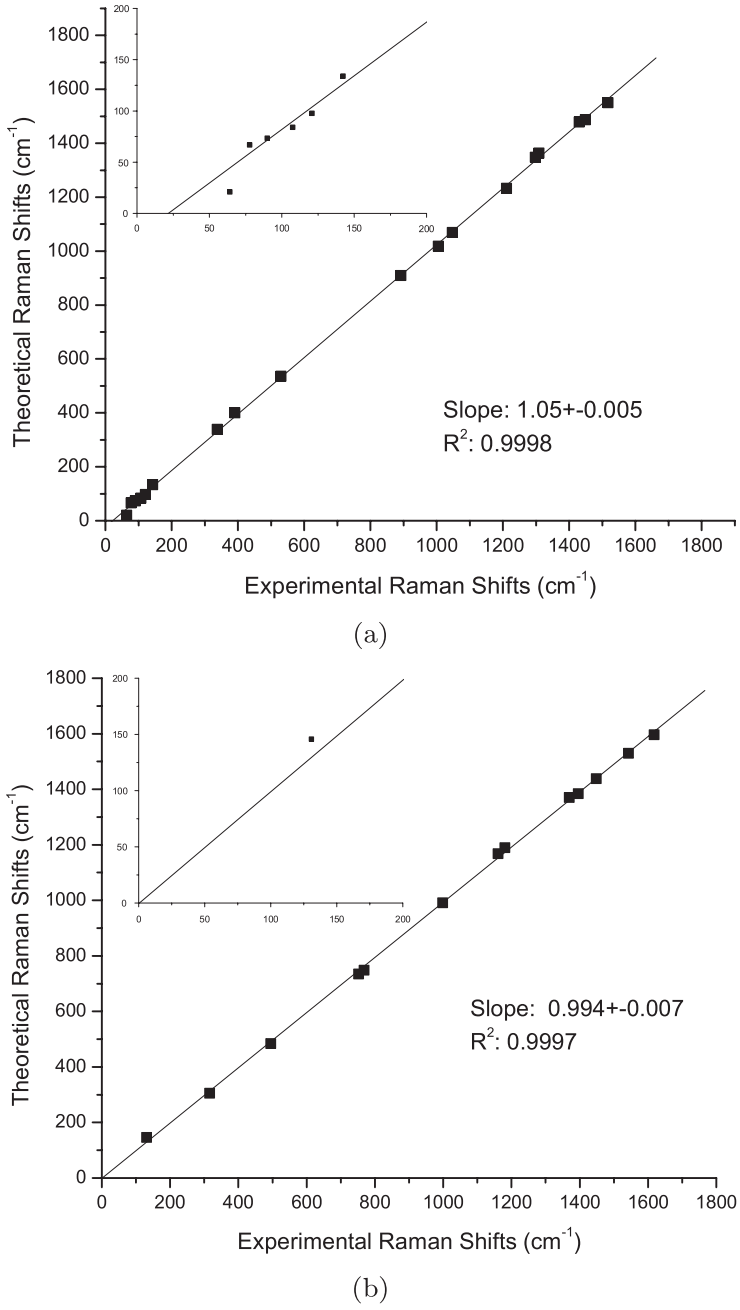

Figure 6. Correspondence between experimentally measured and theoretically calculated peak positions for (a) rubrene and (b) tetracene single crystals. The insets in both graphs are for the low-energy region of the spectra depicted in figure 5.

the molecule also strongly influences the mobility [31]. Also, as expected, under hydrostatic pressure the field-effect hole mobility increases due to an increased π-electron overlap [32].

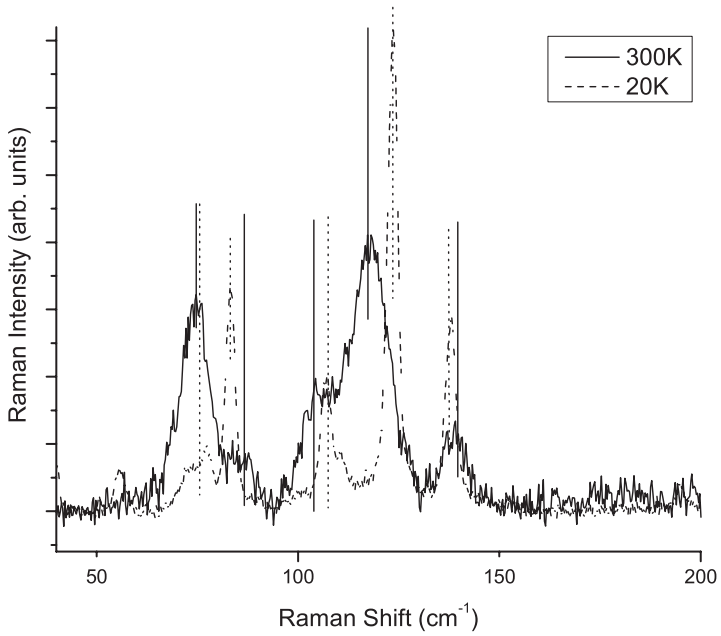

Figure 7. Comparison between low-temperature and room-temperature Raman spectra of rubrene crystals. See table 6 for exact peak positions.

Table 6. Peak positions for rubrene intramolecular modes at 300 and 20 K as displayed in figure 7.

Position (cm^{-1}) 300 K	Position (cm^{-1}) 20 K	Difference (%)
73.7	75.6	2.5
85.7	83.2	−2.9
107.0	107.2	0.2
120.3	123.5	2.7
141.7	138.0	2.6

Measurements of mobility in organic field-effect transistors have been made predominantly on lower-bandgap materials, for which it is easier to fabricate contacts. The high mobilities reported may be as much a result of the small bandgap than of the large π-electron overlap. The measured mobilities to date are, in fact, only lower bounds because of intrinsic factors like traps and defects which can limit the source–drain conductivity and result in a decreased transistor mobility compared to the bulk properties of the material. Additionally, difficulties in making high-quality, low-resistance contacts can lower the measured mobility of a device. Unfortunately, the size of the crystals is typically too small to allow for a four-contact device, so corrections cannot be made for the contact resistance. Other research groups have been able to fabricate four-probe single-crystal FETs and find a high contact-corrected mobility of 8 $cm^2\ V^{-1}\ s^{-1}$ [33]. Regardless of the contacts, however, in an FET structure the transport takes place in a very thin surface layer. This means that measurements of rubrene FETs may show a high mobility in spite of the weak intermolecular interactions because the thin peroxide layer improves the contact to the bulk of the crystal where carrier scattering is limited. The speculation will require more detailed study to explain completely. As previously stated,

Table 7. Densities and mobilities of oligoacenes.

Crystal	Density (g cm^{-3})	Hole mobility (cm^2 V^{-1} s^{-1})	
		Experimental	Theoretical
Napththalene	1.17[a]	1[b]	1.32[c]
Anthracene	1.24[d]	2.1[e]	1.84[a]
Tetracene	1.29[f]	1.3[g]	4.24[a]
Pentacene	1.33[d]	2.2[h]	5.37[a]
Rubrene	1.27	20[i]	

[a] See [35].
[b] See [36].
[c] See [37].
[d] See [38].
[e] See [1].
[f] See [39].
[g] See [40].
[h] See [41].
[i] See [15].

rubrene readily forms an endoperoxide, but this oxidation is limited to a very thin surface layer on a single crystal [34]. Therefore one would not expect a large contribution to the overall bulk Raman signal from the peroxide molecules. Further, simulations of ten different possible peroxide structures yielded results that are not sufficiently different from each other or rubrene to be experimentally distinguishable.

4. Conclusion

Since rubrene is of interest to many researchers for its possible application in devices, a fundamental understanding of the underlying physics that makes the material unique is important. The Raman data indicate that there are very small intermolecular interactions in rubrene. All organic molecular solids are characterized by weak intermolecular bonds, as the van der Waals bonds between molecules are orders of magnitude weaker than the covalent bonds between atoms in a molecule, but rubrene appears to be more of an extreme case than other materials. The intermolecular forces in rubrene are small enough to be not measurable by Raman spectroscopy, or, at least, not observable in these experiments.

Acknowledgments

The authors gratefully acknowledge helpful discussions with Mr Eric Harley and Dr Kristopher McGuire. We also appreciate the help Mr Zhongqiao Ren provided with additional Raman scans of the larger three-dimensional crystallites. We also wish to thank T Segrist for sharing his unpublished x-ray data with us. We are indebted to Mr Jonathan Miller for his implementation of the Perl scripts to generate the animations on the web site cited in this paper. One of the authors (CK) would like to acknowledge the support of the US Department of Energy under Grant No. 04SCPE389. Support for JWW and LM was provided by NSF under grant no. DMR-0505773.

References

[1] Silin'sh E A and Capek V 1994 *Organic Molecular Crystals: Interaction, Localization, and Transport Phenomena* (New York: AIP)
[2] Pope M and Swenberg C E 1982 *Electronic Processes in Organic Crystals* (Oxford: Oxford University Press)

[3] Tang C W and VanSlyke S A 1987 *Appl. Phys. Lett.* **51** 913
[4] Horowitz G 2004 *J. Mater. Res.* **19** 1946
[5] Horowitz G, Garnier F, Yassar A, Hajlaoui R and Kouki F 1996 *Adv. Mater.* **8** 52
[6] Inokuchi H 1985 *Mol. Cryst. Liq. Cryst.* **125** 51
[7] Matsumoto S 1972 *J. Inst. Electron. Commun. Eng. Japan* **55** 397
[8] Uchida M, Adachi C, Koyama T and Taniguchi Y 1999 *J. Appl. Phys.* **86** 1680
[9] Sakamoto G, Adachi C, Koyama T, Taniguchi Y, Merritt C D, Murata H and Kafafi Z H 1999 *Appl. Phys. Lett.* **75** 766
[10] Aziz H and Popovic Z D 2002 *Appl. Phys. Lett.* **80** 2180
[11] Zhilin Z, Xueyin J and Shaohong X 2000 *Thin Solid Films* **363** 61
[12] Hamada Y, Kanno H, Sano T, Fujii H, Nishio Y, Takahashi H, Usuki T and Shibata K 1998 *Appl. Phys. Lett.* **72** 1939
[13] Botzung-Appert E, Monnier V, Duong T H, Pansu R and Ibanez A 2004 *Chem. Mater.* **16** 1609
[14] Arutyunov A S 1982 *Prib. Tekh. Eksp.* **25** 224
[15] Podzorov V, Menard E, Borissov A, Kiryukhin V, Rogers J A and Gershenson M E 2004 *Phys. Rev. Lett.* **93** 086602
[16] Williams W G 1971 *Discuss. Faraday Soc.* **51** 61
[17] Laudise R A, Kloc C, Simpkins P G and Siegrist T 1998 *J. Cryst. Growth* **187** 449
[18] Zeis R, Besnard C, Siegrist T, Schlockermann C, Chi X and Kloc C 2006 *Chem. Mater.* **18** 244
[19] Henn D E, Williams W G and Gibbons D J 1971 *J. Appl. Crystallogr.* **4** 256
[20] Hamada Y, Kanno H, Tsujioka T, Hisakazu T and Usuki T 1999 *Appl. Phys. Lett.* **75** 1682
[21] Ohno K, Mutoh H and Harada Y 1982 *Surf. Sci.* **115** L128
[22] Frisch M J *et al* 2004 *Gaussian 03, revision c.02*
[23] Bulgarovskaya I, Vozzhennikov V, Aleksandrov S and Belsky V 1983 *Zinat. Akad. Vestis, Khim. Ser* **4** 53–9 (Data as cited in the Cambridge structural Database run by the Cambridge Crystallographic Data Centre)
[24] Holmes D, Kumaraswamy S, Matzger A and Vollhardt K 1999 *Eur. J. Org. Chem.* **5** 3399 (Data as cited in the Cambridge Structural Database run by the Cambridge Crystallographic Data Centre)
[25] Sinha P, Boesch S E, Gu C M, Wheeler R A and Wilson A K 2004 *J. Phys. Chem.* A **108** 9213
[26] Maddams W F and Royaud I A M 1990 *Spectrochim. Acta* A **46** 309
[27] Rumi M, Zerbi G, Mullen K, Muller G and Rehahn M 1997 *J. Chem. Phys.* **106** 24
[28] Filippini G and Gramaccioli C M 1984 *Chem. Phys. Lett.* **104** 50
[29] Saleh M 1980 *Phys. Scr.* **21** 220
[30] Horoyski P and Thewalt M 1993 *Phys. Rev.* B **48** 11446
[31] Da Silva Filho D A, Kim E and Bredas J L 2005 *Adv. Mater.* **17** 1072
[32] Rang Z L, Nathan M I, Ruden P P, Podzorov V, Gershenson M E, Newman C R and Frisbie C D 2005 *Appl. Phys. Lett.* **86** 123501
[33] Podzorov V, Sysoev S E, Loginova E, Pudalov V M and Gershenson M E 2003 *Appl. Phys. Lett.* **83** 3504
[34] Ramamurthy V and Venkatesan K 1987 *Chem. Rev.* **87** 433
[35] Abrahams S C, Robertson J M and White J G 1949 *Acta Crystallogr.* **2** 33
[36] Karl N 2003 *Synth. Met.* **133/134** 649
[37] Deng W Q and Goddard W A 2004 *J. Phys. Chem.* B **108** 8614
[38] Mathieson A, Robertson J M and Sinclair V C 1950 *Acta Crystallogr.* **3** 245
[39] Trotter J 1950 *Acta Crystallogr.* **15** 289
[40] Goldmann C, Haas S, Krellner C, Pernstich K P, Gundlach D J and Batlogg B 2004 *J. Appl. Phys.* **96** 2080
[41] Roberson J M, Kowalik J, Tolbert L, Kloc C, Zeis R, Chi X, Fleming R M and Wilkins C 2005 *J. Am. Chem. Soc.* **127** 3069